Microstructural characterization of as-cast high-nitrogen Fe–15Cr–15Ni alloys

J. W. SIMMONS, D. G. ATTERIDGE
Oregon Graduate Institute of Science and Technology, 19600 N.W. Von Neumann Drive, Beaverton, OR 97006, USA

J. RAWERS
Albany Research Center, US Bureau of Mines, 1450 S.W. Queen Avenue, Albany, OR 97321, USA

A base composition of Fe–15Cr–15Ni was melted in a hot-isostatic-pressure furnace under nitrogen pressures from 0.1–150 MPa (1–1500 atm) to produce materials with nitrogen concentrations from 0.04–3.6 wt %. Microstructural characterization of the as-cast materials was completed using optical microscopy, X-ray diffraction, scanning electron microscopy, and transmission electron microscopy techniques. The phases present in the materials were austenite, nitrides (Cr_2N and CrN), and martensite. All of the materials solidified with primary austenite dendrites. Dendritic solidification of CrN occurred in interdendritic regions of the austenite in alloys containing between 0.6 and 1.9 wt % N. Cellular precipitation of Cr_2N occurred in alloys with intermediate nitrogen concentrations (0.6 and 1.0 wt %). The orientation relationship between the Cr_2N and austenite, expressed as $\{1\,1\,1\}\gamma//\{0\,0\,0\,1\}Cr_2N$ and $\langle 1\,1\,0 \rangle\gamma//\langle -1\,1\,0\,0 \rangle Cr_2N$, was confirmed. Precipitates of CrN with both lamellar and disc morphologies formed in the austenite. Both had a cube–cube orientation relationship with the austenite. Only about 10% of the 3.6 wt % N material solidified as primary austenite. The remainder of the material solidified as a eutectic according to the reaction $L \rightarrow \gamma + CrN$. All of the austenite in the eutectic region subsequently transformed to martensite. Increasing volume fractions of martensite formed with increasing bulk nitrogen concentrations in the materials due to alloy depletion of austenite caused by nitride formation.

1. Introduction

Alloying of austenitic stainless steels (SS) with nitrogen instead of carbon has been receiving increased attention recently due to the advantages nitrogen-alloyed materials have with respect to strength, strain hardening, toughness, and pitting corrosion resistance [1–8]. Nitrogen, as an interstitial element, is much more effective than substitutional elements as a solid-solution strengthener, and also surpasses carbon in this respect [9, 10]. Nitrogen has long been used in lower concentrations (< 0.2 wt %) in austenitic SS as an austenite stabilizer to replace nickel and as a strengthening agent instead of carbon. However, in the last 10 years, much higher nitrogen concentrations have been experimented with in austenitic steels. This has resulted in a new class of high-nitrogen austenitic steels (over 0.40 wt % N) [8] which exhibit significantly enhanced mechanical properties as compared to conventional austenitic SS [3, 5–8].

As well as being a potent strengthening agent, nitrogen has a higher solubility in austenitic steels than carbon. This leads to slower precipitation rates for nitrides (versus carbides) in austenitic materials with equal interstitial contents [11–16]. However, this advantage may be lost when ultra-high nitrogen con-

centrations are employed and lead to primary nitride formation, metal/nitride eutectic reactions, and/or solid-state precipitation.

One of the commercial limitations to the use of high-nitrogen alloys is the low solubility of nitrogen in liquid iron alloys at atmospheric pressure [11–14]. As an example, the solubility of nitrogen in an Fe–15Cr–15Ni alloy at 1873 K and atmospheric pressure is only about 0.13 wt % [11, 17]. However, the solubility of nitrogen in liquid alloys increases with increasing nitrogen pressure above the melt in accordance with Sievert's law. That is, the nitrogen concentration in the liquid metal increases as the square root of the nitrogen over-pressure [11–14, 17, 18].

The nitrogen content in iron-based alloys can be increased above the solubility limit at atmospheric pressure by using processing techniques such as pressurized induction melting, plasma remelting, hot isostatic pressure (HIP) melting, and pressurized electroslag remelting (PESR) [17–20]. There is currently commercial production of high-nitrogen steels using PESR in which nitrogen is added directly into the melt via nitrogen-bearing additives such as Cr–N, Fe–Cr–N, Mn–N, and/or Si–N. The other processes mentioned rely on nitrogen pick-up at the interface

between the molten metal and gas through the breakdown of the diatomic nitrogen gas molecule (N_2) to monoatomic nitrogen (N) which is then absorbed into the molten metal. The nitrogen pick-up in this case is time dependent and the processes which rely on this phenomenon can have chemical segregation problems [17, 18, 21].

Research in nitrogen alloying has recently centred around the introduction of greater amounts of nitrogen into austenitic materials. These nitrogen levels greatly exceed the nitrogen solubility in the materials at atmospheric pressure. Such high nitrogen contents can lead to either primary or secondary nitride formation in the melt, or highly supersaturated solutions in which nitride precipitation occurs upon thermal exposure at elevated temperatures for even short periods of time.

In the present study, microstructural development in as-cast Fe–15Cr–15Ni–N alloys with nitrogen contents varying from 0.04–3.6 wt % was characterized and correlated to the phase reactions thought to occur in the quaternary system. The results are explained in terms of the effect of increasing nitrogen concentrations on phase equilibria in the Fe–15Cr–15Ni system.

2. Experimental procedure

High-nitrogen concentrations were achieved by melting individual heats of Fe–15Cr–15Ni base material (0.7 kg) in a HIP furnace under nitrogen pressures of 0.1–150 MPa (1–1500 atm). A typical temperature/pressure versus time profile used during the melting process is shown in Fig. 1. The materials were melted, held under the appropriate nitrogen pressure in the liquid state for at least 1 h, and subsequently furnace cooled under pressure (down to about 1000 °C) at a rate of approximately 20 °C min^{-1}. The total nitrogen concentration of each material was determined with the inert gas-fusion technique using a Leco nitrogen–oxygen determinator, Model TC 436.

The crystal phases present in the materials were initially identified using X-ray diffraction (XRD) analysis (CuK_α radiation). The microstructures of the as-cast materials were characterized using optical micro-

scopy after etching with one of the following solutions; (1) 10 ml HNO_3, 10 ml HCl, 10 ml glacial acetic acid, and 2 drops glycerol, or (2) electrolytically with 10% oxalic acid. Three-dimensional morphologies of the nitride phases were characterized by examining metallographically prepared sections of the materials in a scanning electron microscope (SEM) after etching with a 10% bromine/methanol solution.
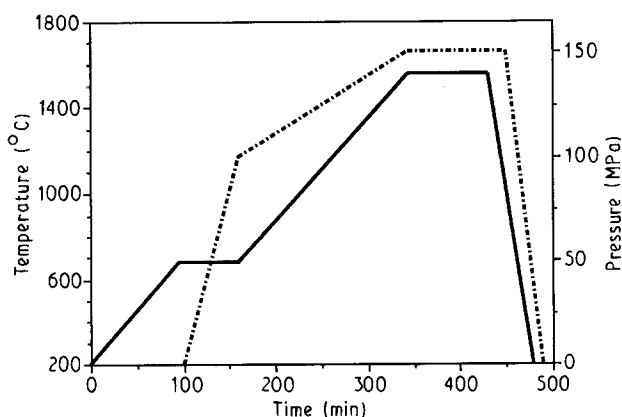
Microstructures present in 0.6, 1.0, 1.9, and 3.6 wt % N materials were examined in detail using transmission electron microscopy (TEM). Specimens for TEM were sectioned from each material, ground to 50–100 μm thickness, dimpled using 3 μm diamond paste, ion milled, and subsequently characterized using a Hitachi H800 analytical electron microscope. Specimens from the high-nitrogen materials could not be successfully prepared using the twin-jet electropolishing technique due to the high volume fraction of nitrides present. Standard selected-area diffraction pattern (SADP) analysis techniques were used to identify crystal phases in the TEM. Careful measurement of interplanar spacings was carried out using camera constants determined with a gold standard under identical instrument conditions. In addition, all of the diffraction patterns generated were compared to computer-generated diffraction patterns using known camera constants and assumed crystal structures of the phases being identified.

3. Results and discussion
3.1. Phases, microstructures and morphologies
The phases and the phase morphologies observed in the five Fe–15Cr–15Ni cast alloys with nitrogen concentrations varying from 0.04–3.6 wt % are summarized in Table I. These results were compiled using XRD, optical microscopy, SEM, and TEM examinations. In Table I, the phase with the greatest volume fraction is listed first with the remaining phases listed in decreasing order of concentration. Austenite was the primary solidification phase for all of the nitrogen compositions studied. The other phases present in the materials were chromium nitrides (Cr_2N and CrN). and martensite. The π phase (B-manganese structure), described by Kikuchi et al. [21, 22] to be the equilibrium nitride in high chromium–high nickel austenitic steels, was not present in any of the materials. This is not unexpected because Kikuchi et al. described Cr_2N as an intermediate precipitate which transforms to the π phase after long ageing times at temperatures between approximately 700 and 1000 °C.

The Cr_2N has a hexagonal crystal structure with lattice parameters of $a = 0.481$ nm and $c = 0.448$ nm, a c/a ratio of 0.932, and belongs to the space group P-31m. The lattice parameters of Cr_2N vary as a function of the nitrogen concentration in the nitride which has been reported to be between 11.3 and 11.9 wt % (32 and 33.3 at %). The stoichiometry of CrN reportedly does not vary and contains considerably more nitrogen at 21.2 wt % (50 at %). The

Figure 1 Schematic temperature (———)/pressure (—·—) versus time profile for melting and solidification in the hot isostatic pressure furnace.

TABLE I Nitrogen contents, phases and phase morphologies present in Fe–15Cr–15Ni–N alloys

Alloy (wt % N)	Phases present[a]	Morphology
0.04	γ	Primary dendrites – single-phase material
0.60	γ	Primary dendrites
	Cr_2N	"False pearlite" at austenite grain boundaries
	CrN	Secondary dendrites at austenite interdendritic regions
	α'	Present at γ/CrN interfaces
1.0	γ	Primary dendrites
	CrN	Secondary dendrites at austenite interdendritic regions
	Cr_2N	Lamellar precipitates in austenite interdendritic regions
	CrN	Micro-precipitates in austenite
	CrN	Lamellar precipitates in austenite interdendritic regions
	α'	Present at γ/CrN interface regions
1.9	γ	Primary dendrites
	CrN	Secondary dendrites at austenite interdendritic regions
	CrN	Micro-precipitates in austenite
	α'	Present at γ/CrN interface regions
3.6	α'	Transformed from austenite in γ/CrN eutectic regions
	CrN	Part of eutectic solidification (L $\rightarrow \gamma$ + CrN)
	γ	Primary dendrites

[a] γ = austenite (f c c), α' = martensite (b c c).

CrN has the cubic NaCl structure with a lattice parameter of $a = 0.414$ nm [23–25].

Optical micrographs, representative of the microstructures of the as-cast Fe–15Cr–15Ni materials, are shown in Figs 2–5. The nitride morphologies characteristic of these materials are illustrated by secondary electron micrographs (Figs 2–5). As mentioned previously, the micrographs were taken after the specimens were etched with a 10% bromine/methanol solution which preferentially attacked the austenite and left the nitrides in relief, thus showing their three-dimensional structure.

The magnetic properties of the materials increased with increasing nitrogen content. The 0.04 wt % N material was totally non-magnetic, while all of the alloys with nitrogen contents of 0.6 wt % and greater were magnetic, with the 3.6 wt % alloy showing the strongest magnetic properties. These observations, coupled with XRD results, revealed the presence of increasing martensite/ferrite volume fractions in the alloys with increasing nitrogen contents.

The Fe–15Cr–15Ni material containing 0.04 wt % N had a single-phase structure consisting of austenite. No nitrides were observed in this material. The material containing 0.60 wt % N consisted of primary austenite dendrites, but also contained the chromium nitrides Cr_2N and CrN. The Cr_2N nucleated at austenite grain boundaries and precipitated with a lamellar morphology into adjacent austenite grains (Fig. 2a–c). The resulting cellular structure (austenite + Cr_2N) has been referred to as "false pearlite" due to its resemblance to pearlite in carbon steels. However, this Cr_2N formation does not occur as part of an eutectoid reaction, but results from the discontinuous (cellular) decomposition of austenite, according to the reaction $\gamma_1 \rightarrow \gamma_2 + Cr_2N$ [26, 27]. Dendritic solidification of CrN occurred in a few isolated austenite interdendritic regions of this material. This is illustrated in the scanning electron micrograph of Fig. 2d in

which a dendrite of CrN is shown surrounded by lamellar Cr_2N.

The cellular precipitation of Cr_2N in high-nitrogen Fe–Cr–Ni austenitic steels has been reported by many researchers. Kajihara et al. [26] applied a model for discontinuous precipitation of binary substitutional alloys by Hillert [28] to the cellular precipitation of Cr_2N. It was assumed that the diffusivity of nitrogen was infinite and the boundary diffusion of chromium along the moving cell boundary was the rate-controlling process. The primary features of the cellular precipitation of Cr_2N in austenite can be summarized as follows. The growth of cells consisting of lamellar Cr_2N and transformed austenite takes place by the long-range diffusion of nitrogen into the cell from the untransformed matrix. This leads to a decrease in the nitrogen supersaturation in the untransformed matrix, a decrease in the driving force for precipitation, and therefore a decrease in the rate of cell-boundary migration. The cell boundary ceases to migrate even though the untransformed matrix is still supersaturated with nitrogen. The total nitrogen concentration within a cell region (austenite and Cr_2N) is greater than that of the initial untransformed matrix [27].

The 1.0 wt % N material had two regions with slightly varying microstructural features which were most likely created as a result of nitrogen segregation in the melt. These two regions are illustrated in the optical and secondary electron micrographs of Fig. 3. Both regions consisted of primary austenite dendrites, dendritic CrN located in austenite interdendritic regions, and lamellar Cr_2N. However, in the first region, shown in Fig. 3a and b, CrN micro-precipitates formed in the austenite just outside of the interdendritic CrN. The scanning electron micrograph of Fig. 3b illustrates the very high density of CrN precipitates present in this region and the precipitate-free zone (pfz) between them and the dendritic CrN. The
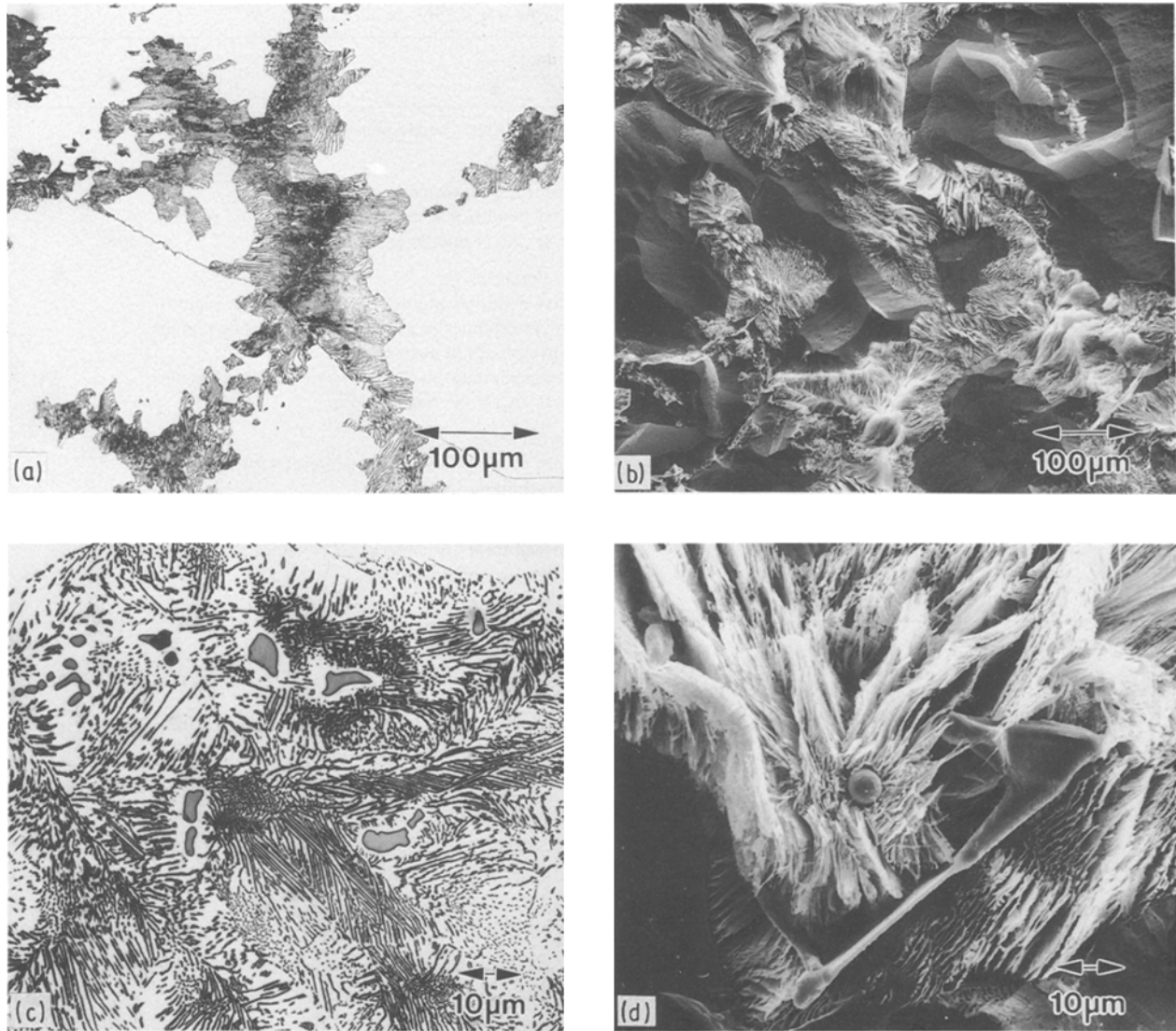
Figure 2 0.6 N (wt %) alloy. (a, c) Optical micrographs showing the lamellar structure of the cellular decomposition products (austenite + Cr_2N). (b, d) Scanning electron micrographs of (b) lamellar Cr_2N and (d) lamellar Cr_2N/secondary CrN dendrite.

Cr_2N was present outside of the micro-precipitates in austenite/Cr_2N cells formed by cellular decomposition of the primary austenite, similar to the 0.60 wt % N material. No CrN micro-precipitates were observed in the second region (Fig. 3c and d). However, along with the presence of lamellar Cr_2N in this region, lamellar CrN was also observed. The lamellar CrN structure is discussed in Section 3.2.

The 1.9 wt % N material contained more dendritic CrN, located in the austenite interdendritic regions, than the lower nitrogen materials (Fig. 4a). The dendritic nature of this CrN is illustrated by the secondary electron micrograph of Fig. 4b. This material also contained CrN micro-precipitates which formed in the austenite just outside the interdendritic CrN. The CrN micro-precipitates in this sample were identical to those in the 1.0 wt % N material. No Cr_2N was present in this material.

The microstructure typical of the 3.6 wt % N alloy is shown in the optical micrograph of Fig. 5a. The microstructure consisted of primary austenite dendrites and a two-phase CrN/martensite structure. The

CrN took on a rod-like morphology in this material as shown in the secondary electron micrograph of Fig. 5b. This suggests eutectic solidification took place in the remaining liquid, after primary austenite formation, according to the reaction $L \rightarrow \gamma + CrN$. The austenite, destabilized by low chromium and nitrogen levels, then transformed to martensite upon further cooling of the material. The presence of the martensite is illustrated by the TEM results in the next section. As with the 1.9 wt % N alloy, no Cr_2N was detected in this material.

3.2. TEM examinations
The lamellar structure of the Cr_2N in the 0.6 and 1.0 wt % N materials is illustrated in the bright-field (BF) transmission electron micrographs of Fig. 6a and b, respectively. A typical selected-area diffraction pattern (SADP) taken from the austenite/Cr_2N region of Fig. 6b is shown in Fig. 6c. The SADP of Fig. 6c is a [1 1 0] zone axis (ZA) of the austenite matrix (bright spots) and a [− 1 1 0 0] ZA of Cr_2N. For this and
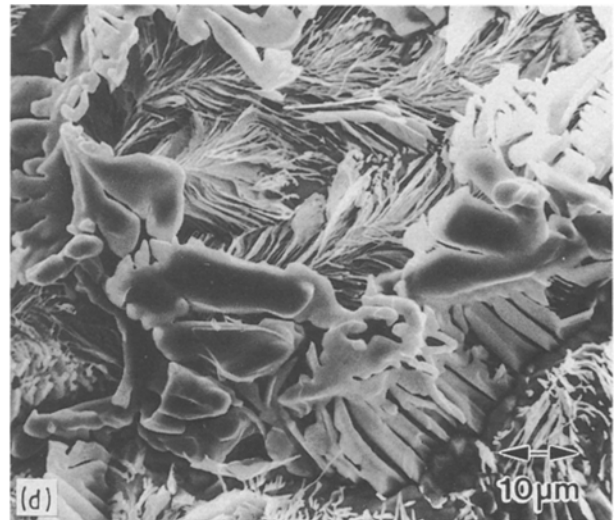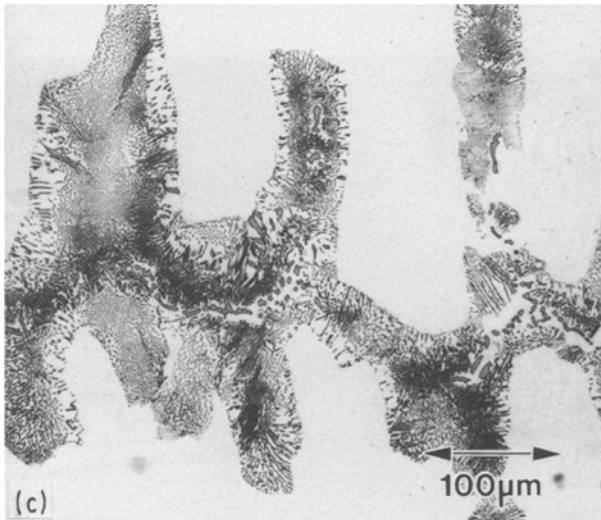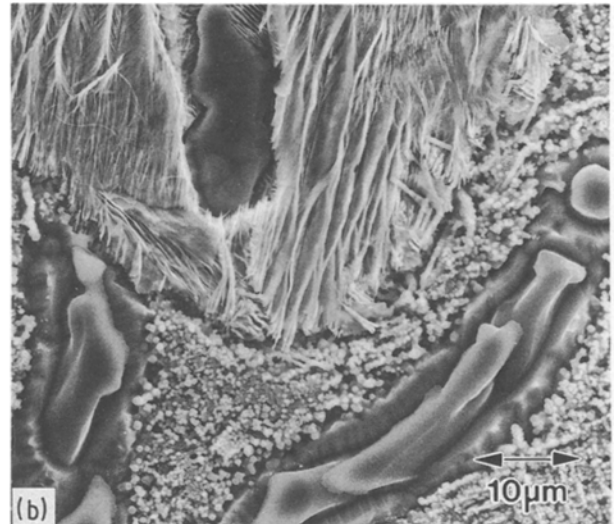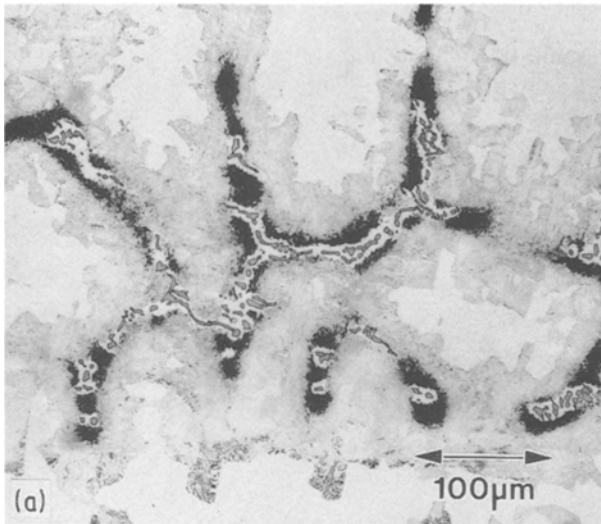
Figure 3 Optical and scanning electron micrographs from two regions of the 1.0 N (wt %) material. The first region (a, b) consisted of primary austenite, dendritic CrN, lamellar Cr_2N, and CrN micro-precipitates. The second region (c, d) consisted of primary austenite, dendritic CrN, lamellar Cr_2N, and lamellar CrN.
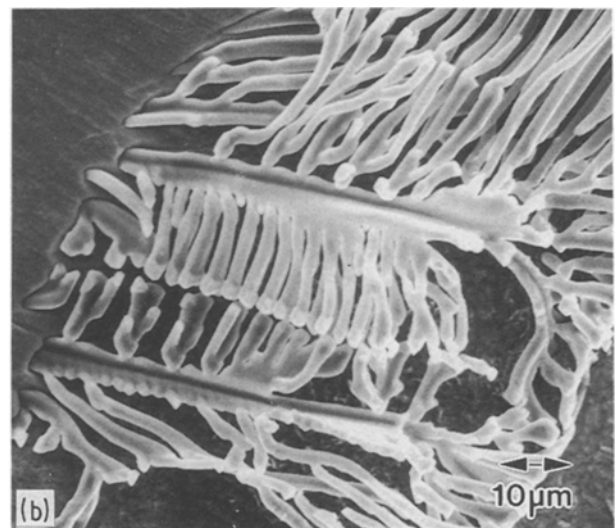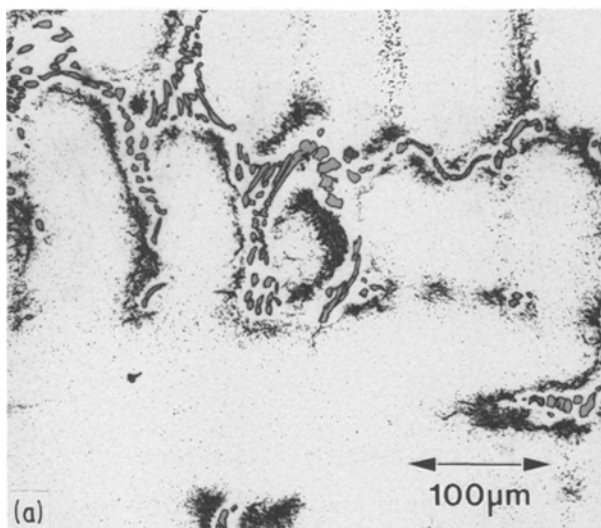
Figure 4 1.9 N (wt %) alloy. (a) Optical micrograph showing primary austenite dendrites, secondary CrN dendrites (grey), and CrN micro-precipitates (black regions). (b) Scanning electron micrograph illustrating the dendritic nature of the CrN (grey phase in (a)).
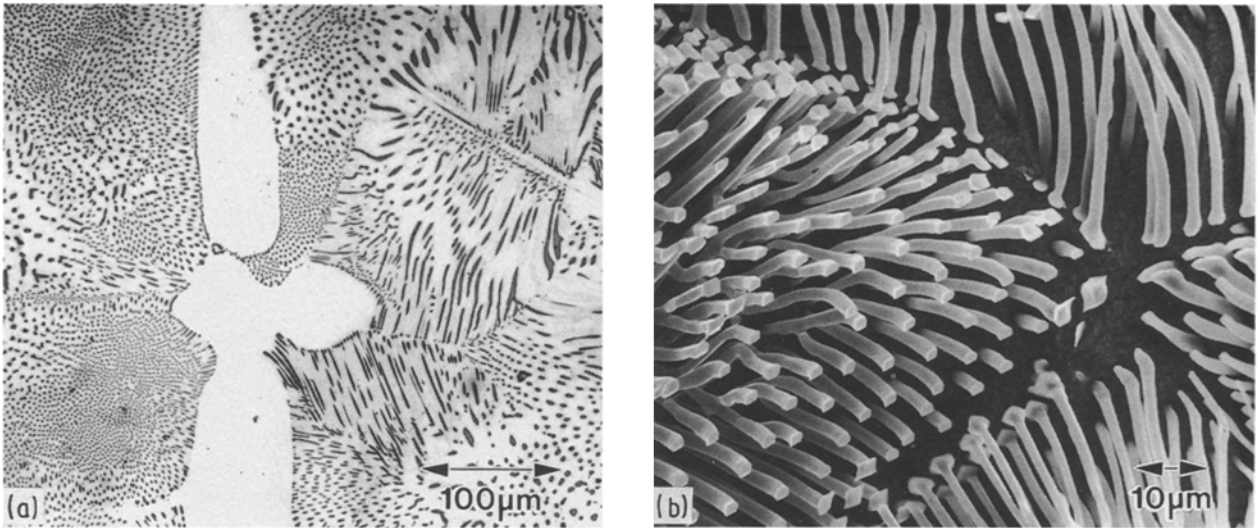
Figure 5 3.6 N (wt %) alloy. (a) Optical micrograph of primary austenite dendrites and a two-phase CrN/martensite structure (see text). (b) Scanning electron micrograph showing the rod-like morphology of the CrN.

○ γ (fcc) matrix, [110] zone

• Cr₂N (hcp) precipitate [$\bar{1}$100] zone
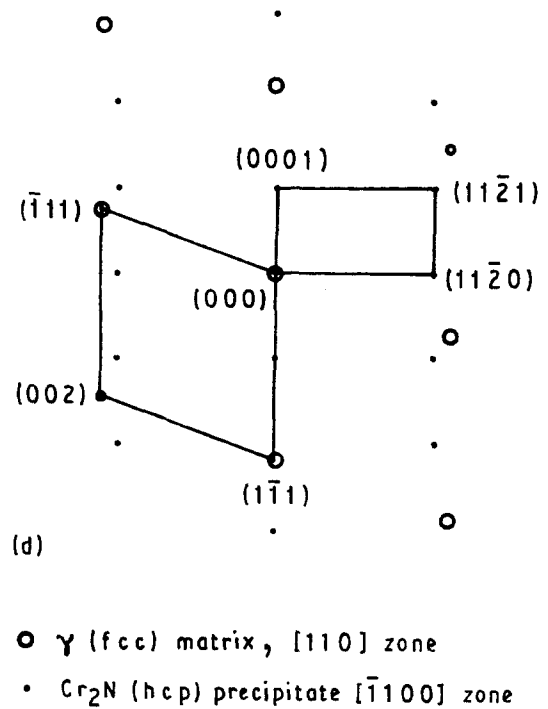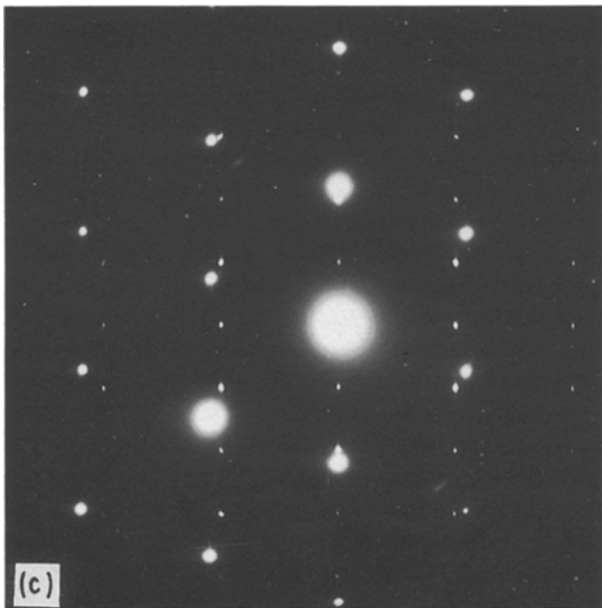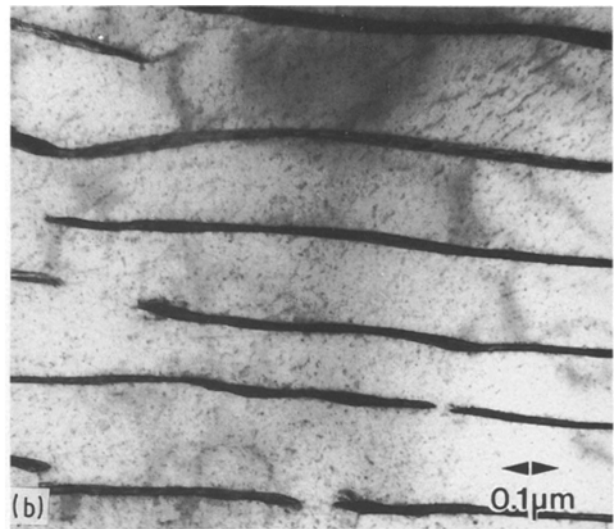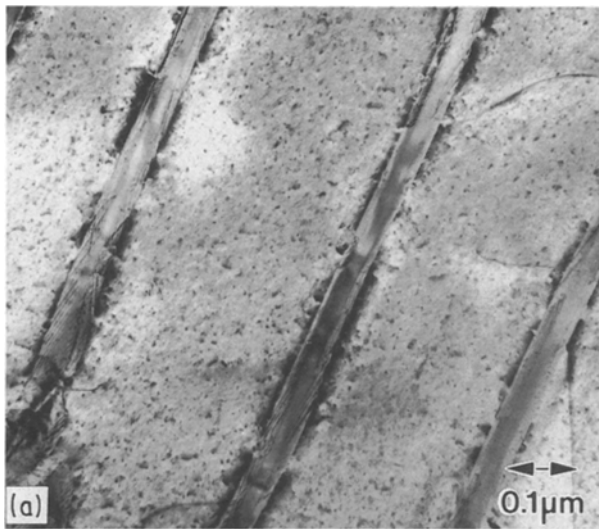
Figure 6 BF transmission electron micrographs of lamellar Cr_2N/austenite from the (a) 0.6 N (wt %) and (b) 1.0 N (wt %) materials. (c) SADP from area shown in (b), and (d) schematic representation of the SADP.

other diffraction patterns analysed, the basal plane $\{0\,0\,0\,1\}$ of the Cr_2N was parallel to the $\{1\,1\,1\}$ of the austenite matrix. These results were confirmed with numerous diffraction patterns taken from austenite/ Cr_2N regions in both the 0.6 and 1.0 wt % N materials. The orientation relationship between the Cr_2N and austenite in the materials of this study corresponds to that reported by Rayaprolu and Hendry [27], expressed as $\{1\,1\,1\}\gamma//\{0\,0\,0\,1\}Cr_2N$ and $\langle 1\,1\,0\rangle\gamma//\langle -1\,1\,0\,0\rangle Cr_2N$.

The diffraction pattern of Fig. 6c is shown schematically in Fig. 6d which was constructed using the orientation relationship between the austenite and Cr_2N described above. As stated by Rayaprolu and Hendry, this orientation relationship is consistent with the close packed planes of the f c c austenite and hexagonal Cr_2N being parallel. The morphological characteristics (i.e. width, spacing, and continuity) of the Cr_2N lamellae varied from region to region in the 0.6 and 1.0 wt % N materials, but no crystallographic differences between these regions could be determined from the TEM results. Variations in the stoichiometry or lattice parameters of the Cr_2N were not determined. Formation characteristics of the austenite/ Cr_2N cells were most likely controlled by local chemistry and thermal effects.

The lamellar CrN observed in the 1.0 wt % N material was located in a twinned region of the austenite matrix as shown in the transmission electron micrographs of Fig. 7. In all diffraction patterns taken from this region of the sample, the reflections from the austenite matrix and CrN lamellae were completely symmetric. Observation of several different zone axes indicated that the austenite matrix and lamellar CrN precipitates had a cube–cube orientation relationship. This is illustrated in the [1 1 0] and [1 1 2] ZA patterns of Fig. 7c and e, respectively. The CrN lamellae were located at twin–matrix interfaces, completely within the matrix, and also crossed twin boundaries. Thus, although the CrN lamellae were parallel to the twin boundaries, they apparently did not nucleate at twin–matrix boundaries. This was the only region in any of the materials where significant twinning of the austenite was observed.

The transmission electron micrographs of Fig. 8 show CrN micro-precipitates typical of those found in the 1.0 and 1.9 wt % N materials. The precipitates were disc shaped and ranged in size from approximately 0.1–0.5 µm. The CrN micro-precipitates exhibited the same cube–cube orientation relationship with the austenite matrix as the CrN lamellae (Fig. 8c and e). The austenite regions containing the CrN micro-precipitates were more highly dislocated than the austenite outside those regions. This is not unexpected, considering the high density of the CrN precipitates and the volume strain energy generated by the precipitation process.

It was stated earlier that the martensite/ferrite content of the materials increased with increasing nitrogen as evinced by XRD results and the changes in the magnetic properties of the materials. The transmission electron micrograph of Fig. 9, taken from the 1.9 wt % N material, shows dendritic CrN located in a primary austenite interdendritic region. The CrN in this material was bounded by a layer of martensite (labelled α' in the micrograph of Fig. 9). Outside of the martensite/CrN region, the material was entirely austenitic. The martensite in this and other samples, identified by selected-area diffraction, had very high dislocation densities with some twinning also observed. In the materials containing 0.6 and 1.0 wt % N, layers of martensite surrounding the dendritic CrN, typically thinner than those found in the 1.9 wt % N material, were also observed.

In the material containing 3.6 wt % N, all of the austenite in the structure that appeared to have formed as a result of a eutectic reaction $(L \rightarrow \gamma + CrN)$ transformed to martensite. The only remaining austenite in this material was the primary austenite dendrites and isolated blocks of retained austenite located within the martensite/CrN structure. The transmission electron micrograph of Fig. 10 was taken from the eutectic region of the 3.6 wt % N material and shows the rod-like CrN (in cross-section) and the surrounding lath martensite structure.

Increasing volume fractions of CrN in the materials resulted in corresponding increases in martensite contents. Martensite formation in the 0.6, 1.0 and 1.9 wt % N materials was restricted to the interfacial regions between CrN dendrites and the surrounding austenite. The martensite most likely formed as a result of two phenomena, depletion of alloying elements (primarily chromium and nitrogen) at the interfacial regions which destabilized the austenite, and strain-induced transformation due to differences in the thermal expansion coefficients of CrN and austenite. Although alloy depletion is considered to be primary, both effects would be expected to increase with increasing volume fractions of CrN and result in increased martensite formation, as observed.

In the 3.6 wt % N material, the martensite was likely formed primarily as a result of decreasing austenite stability due to the depletion of alloying elements (primarily chromium, but probably also nitrogen) caused by the formation of large volume fractions of CrN. This material contained about 18%–20% (by volume) CrN. Thus, it can be estimated that the chromium content in the remaining austenite was reduced to between 5 and 6 wt %. It is expected that a reduction in chromium levels of this magnitude would have a significant effect on the stability of the austenite.

3.3. Microstructural development

Primary austenite solidification of Fe–15Cr–15Ni alloys is predicted at very low concentrations of nitrogen, which is a powerful austenite stabilizer, because the nickel content of the alloy is high. Chromium is expected to be rejected into the melt during solidification of primary austenite dendrites resulting in chromium enrichment in the remaining liquid [29]. It is suggested that in the alloys of the current study nitrogen was also rejected into the melt during solidification. The evidence for this is the notable lack of nitride precipitates in primary austenite

(d)
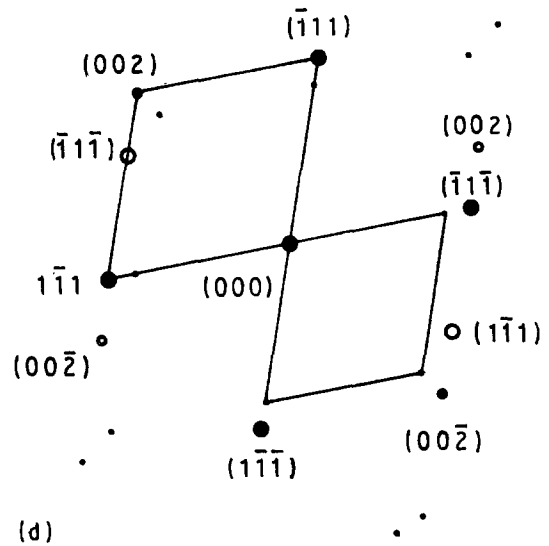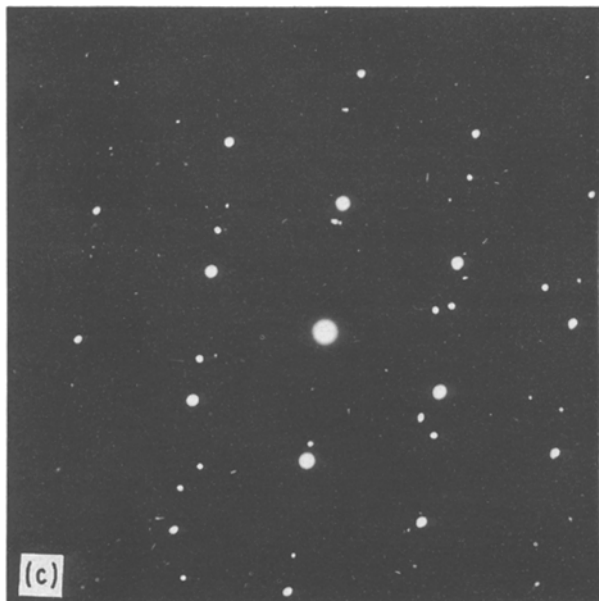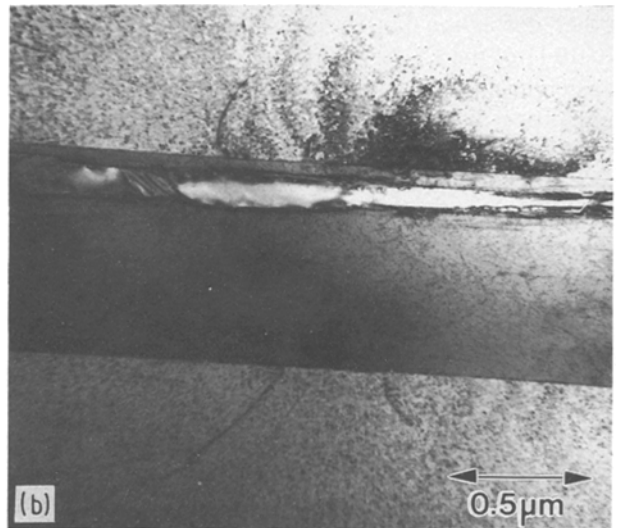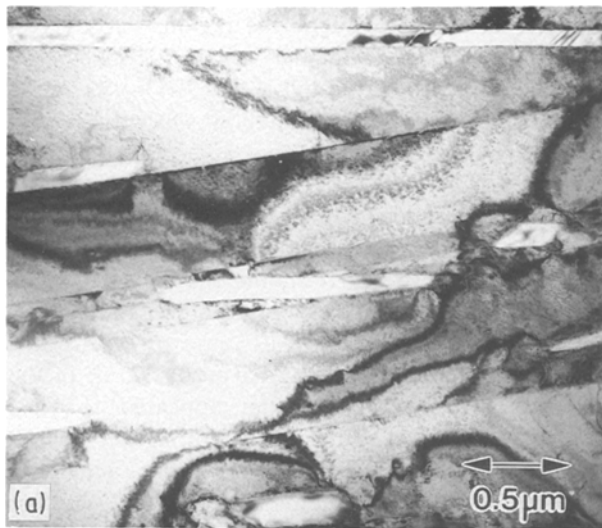
● γ (fcc) matrix , [110] zone

○ γ twin reflections

· CrN (fcc) precipitate [110] zone

Figure 7 (a, b) BF transmission electron micrographs of CrN lamellae in twinned austenite of 1.0 N (wt %) material. (c) SADP and (d) corresponding schematic diagram from twinned austenite/CrN region. (e) SADP [1 1 2] zone axis (austenite matrix outside bright spots, inside spots are from CrN and double diffraction) from CrN/austenite.

dendrites, except at interdendritic regions. This indicates that the nitrogen content in the primary austenite dendrites was much lower than in the interdendritic regions. Dendritic solidification of CrN occurred in the austenite interdendritic regions and the solid-state

precipitation reactions also took place in these regions of high chromium and nitrogen concentrations. Even in the alloy which contained a bulk nitrogen concentration of 3.6 wt % and a volume fraction of CrN around 20%, no precipitation of nitrides occurred in the primary austenite dendrites during cooling. These observations contradict literature reports that the nitrogen solubility in the austenite of Fe–Cr–Ni materials is greater than that in the liquid [22].

The effect of nickel in the present alloy system is basically one of stabilizing and increasing the austenite phase field. Second phases involving nickel were not expected to be present in the materials of this
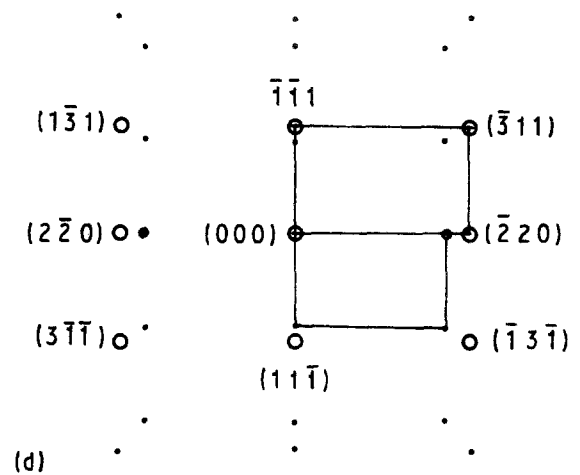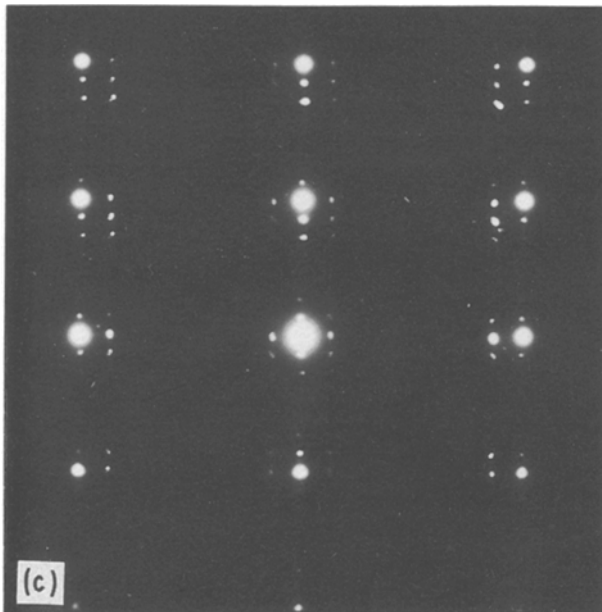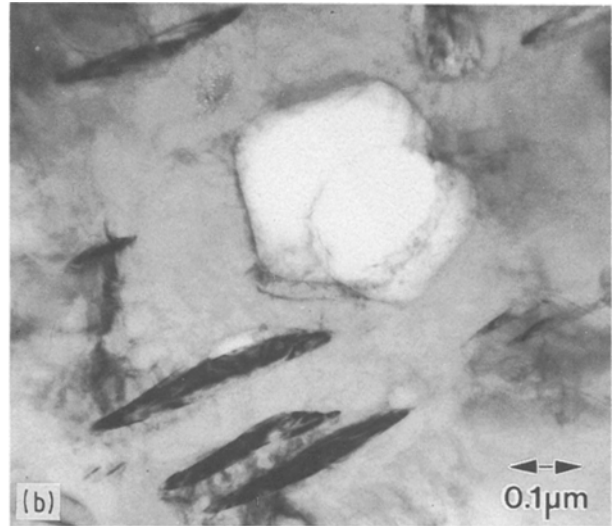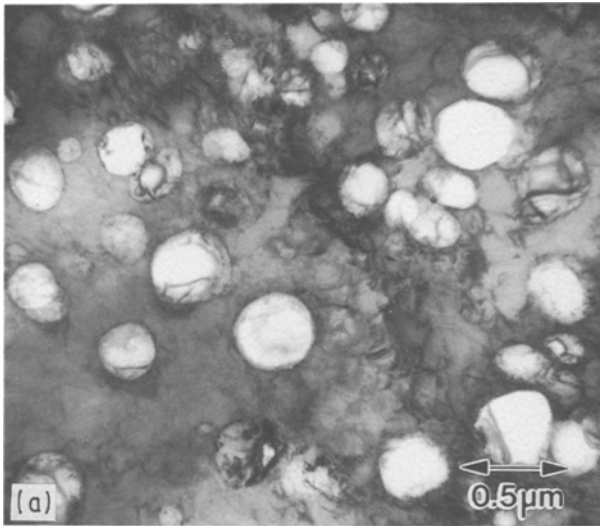
O γ (fcc) matrix [112] zone

• CrN (fcc) precipitate [112] zone
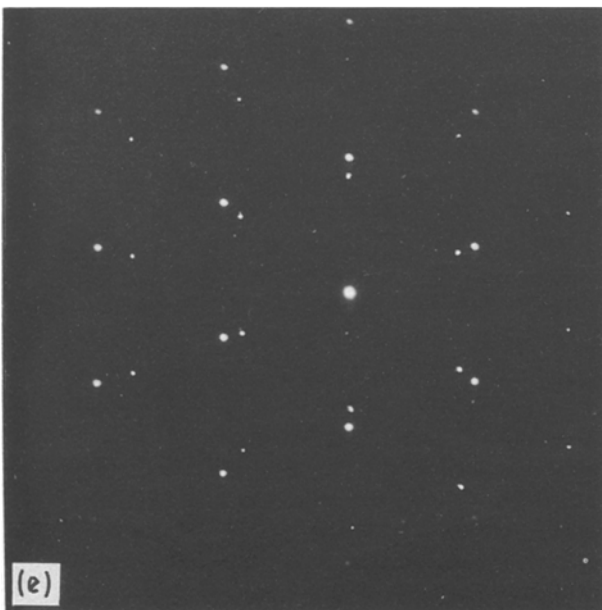
Figure 8 (a, b) BF transmission electron micrographs of austenite/CrN micro-precipitate region (1.0 and 1.9 wt% N alloys). (c) SADP from a region similar to (a) and (d) corresponding schematic diagram showing matching [1 1 2] zones of austenite (fcc) and CrN (fcc), and spots due to double diffraction. (e) An additional SADP [1 1 0] zone (austenite matrix outside bright spots, inside spots from CrN).

study, and none were observed. Therefore, it is assumed that the ternary Fe–Cr–N system can be used to predict microstructural formation in the Fe–Cr–Ni–N system keeping in mind the significant role of nickel in altering phase fields but probably not the reactions themselves.

A pseudo-phase diagram, constructed for the current alloy system and developed from the work of Frisk and Hillert [30], is presented in Fig. 11 as an explanation of the microstructural development in the present alloys. All of the alloys passed through a two-phase L + γ field first, after which either solidification completed as austenite, or a three-phase field (L + γ + CrN) was entered. The final microstructures developed due to alloy segregation which resulted from
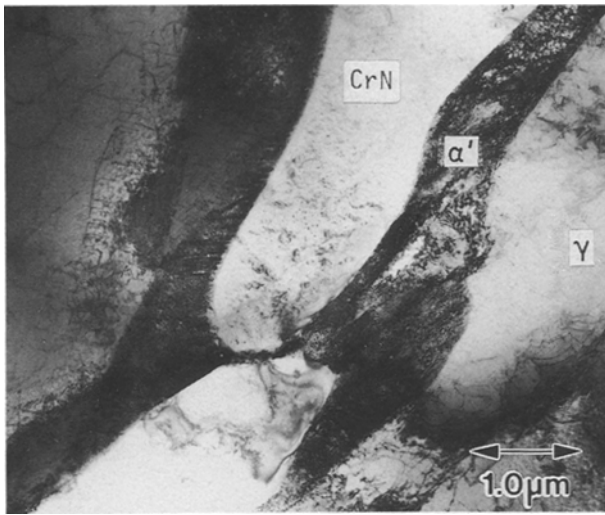
Figure 9 1.9 N (wt %) alloy. BF transmission electron micrograph taken from interdendritic region of primary austenite and showing dendritic CrN bounded by martensite (dark areas, labelled α′) and austenite (γ).

Figure 11 Pseudo-phase diagram constructed for the current Fe–15Cr–15Ni–N alloy system, developed from the work of Frisk and Hillert [30].

Figure 10 3.6 N (wt %) alloy. BF transmission electron micrograph showing cross-section of rod-like CrN and lath martensite.

the rejection of chromium and nitrogen from the austenite during primary solidification. Solid-state precipitation of nitrides subsequently occurred in the enriched regions of the austenite during cooling. The diagram presented in Fig. 11 is obviously over-simplified and neglects the possibility of the alloys having intersected a four or five phase plane, or the presence of a four-phase field. However, the proposed pseudo-phase diagram does explain the current results if segregation effects and alloy rejection from the austenite are taken into account.

4. Conclusion

The microstructural development of cast Fe–15Cr–15Ni–N alloys with nitrogen contents ranging from 0.04–3.6 wt %, melted and solidified under high nitrogen pressures, has been characterized. As-expected,

the volume fraction of chromium-rich nitrides in the materials increased with increasing bulk nitrogen concentrations. A pseudo-phase diagram (Fig. 11) was developed from the work of Frisk and Hillert [30] to explain the microstructural development in the current alloy system.

Primary austenite solidification occurred in all of the Fe–15Cr–15Ni alloys studied. Dendritic solidification of CrN (cubic, NaCl structure) occurred in interdendritic regions of the primary austenite in alloys with 0.6, 1.0 and 1.9 wt % N. Increasing martensite contents were present in the alloys as a function of increasing volume fractions of CrN. Martensite formation in the 0.6, 1.0 and 1.9 wt % N materials was restricted to the interfacial regions between CrN dendrites and the surrounding austenite. The transformations likely occurred as a result of two phenomena, the primary one being the depletion of alloying elements (primarily chromium and nitrogen) at interfacial regions which destabilized the austenite. The other possibility that should be considered is strain-induced transformation due to differences in the thermal expansion coefficients of CrN and austenite.

Cellular precipitation of Cr_2N (hexagonal crystal structure, P-31m space group) occurred in the austenite of alloys with 0.6 and 1.0 wt % N. The Cr_2N nucleated at austenite grain boundaries (interdendritic regions in 1.0 wt % N alloy) and precipitated with a lamellar morphology into adjacent austenite grains. This Cr_2N formation resulted from the discontinuous (cellular) decomposition of austenite, according to the reaction $\gamma_1 \rightarrow \gamma_2 + Cr_2N$ [26, 27]. The orientation relationship obtained between the Cr_2N and austenite, expressed as $\{1\,1\,1\}\gamma//\{0\,0\,0\,1\}Cr_2N$ and $\langle 1\,1\,0 \rangle\gamma//\langle -1\,1\,0\,0 \rangle Cr_2N$, corresponded to that reported in the literature [27]. In addition to lamellar Cr_2N, the 1.0 wt % N material contained CrN which

precipitated in two morphologies, disc-shaped micro-precipitates varying in size from about 0.1–0.5 μm, and lamellar CrN. Both forms of CrN had cube–cube orientation relationships with the austenite.

Materials with nitrogen contents of 1.9 and 3.6 wt % did not contain the Cr_2N nitride, but contained large volume fractions of CrN. Along with the dendritic solidification of CrN in primary austenite inter-dendritic regions of the 1.9 wt % N alloy, high-density areas of CrN micro-precipitates formed which were identical to those in the 1.0 wt % N material.

Primary austenite solidification in the material containing 3.6 wt % N comprised only about 10% of the material volume. The remainder of the material solidified as a eutectic according to the reaction $L \rightarrow \gamma$ + CrN. The CrN in this material had a distinct rod-like morphology. All of the austenite in the eutectic region subsequently transformed to martensite due to the depletion of alloying elements (primarily chromium, but probably also nitrogen) caused by the formation of large volume fractions of CrN (approximately 18%–20% by volume).

Acknowledgements

References

1. M. L. G. BYRNES, M GRUJICIC and W. S. OWEN, *Acta Metall.* **35** (1987) 1853.
2. R. P. REED, *J. Metals* March (1989) 16.
3. E. WERNER, *Mater. Sci. E. A* **101** (1988) 93.
4. N. ARIT, C. GILLESSEN and W. HEIMANN, in "Proceedings of the 2nd International Conference on High Nitrogen Steels, HNS 90", Aachen, Germany, October 1990, edited by G. Stein and H. Witulski (Stahleisen Dusseldorf, 1990) p. 150.
5. P. J. UGGOWITZER and M. O. SPEIDEL, *ibid.*, p. 156.
6. J. MENZEL, G. STEIN and P. DAHLMANN, in "Proceedings of the International Conference on High Nitrogen Steels, HNS 88", Lille, France, May 1988, edited by J. Foct and A. Hendry (The Institute of Metals, London, 1989) p. 147.
7. A. KENDAL, J. E. TRUMAN and K. B. LOMAX, *ibid.*, p. 405.
8. M. O. SPEIDEL, *ibid.*, p. 92.
9. K. J. IRVINE, D. T. LLEWELLYN and F. B. PICKERING, *J. Iron Steel Inst.* **199** (1961) 153.
10. K. J. IRVINE, T. GLADMAN and F. B. PICKERING, *ibid.* **207** (1969) 1017.
11. R. D. PEHLKE and J. F. ELLIOTT, *Trans. Metall. Soc. AIME* **218** (1960) 1088.
12. P. H. TURNOCK and R. D. PEHLKE, *ibid.* **236** (1966) 1540.
13. W. M. SMALL and R. D. PEHLKE, *ibid.* **242** (1968) 2501.
14. H. FEICHTINGER, A. SATIR-KOLORZ and Z. XIAO-HONG, in "Proceedings of the International Conference on High Nitrogen Steels, HNS 88", Lille, France, May 1988, edited by J. Foct and A. Hendry (The Institute of Metals, London, 1989) p. 75.
15. M. DEIGHTON, *J. Iron Steel Inst.* November (1970) 1012.
16. J. GORDON PARR and A. HANSON, "An Introduction to Stainless Steel", revised by R. A. Lula, Consultant (American Society for Metals, Metals Park, OH, 1986).
17. J. MENZEL, G. STEIN and P. DAHLMANN, in "Proceedings of the 2nd International Conference on High Nitrogen Steels, HNS 90", Aachen, Germany, October 1990, edited by G. Stein and H. Witulski (Stahleisen, Dusseldorf, 1990) p. 365.
18. K. FORCH, G. STEIN and J. MENZEL, *ibid.*, p. 258.
19. J. RAWERS, J. DUNNING and R. REED, *ibid.*, p. 63.
20. G. STEIN, J. MENZEL and H. DORR, in "Proceedings of the International Conference on High Nitrogen Steels, HNS 88", Lille, France, May 1988, edited by J. Foct and A. Hendry (The Institute of Metals, London, 1989) p. 32.
21. M. KIKUCHI, T. SEKITA. S. WAKITA and R. TANAKA, *J. Iron Steel Inst. Jpn* **64** (1978) 76.
22. M. KIKUCHI, M. KAJIHARA and K. FRISK, in "Proceedings of the International Conference on High Nitrogen Steels, HNS 88", Lille, France, May 1988, edited by J. Foct and A. Hendry (The Institute of Metals, London, 1989) p. 63.
23. M. HANSEN (ed.), "Constitution of Binary Alloys" (McGraw-Hill, New York, 1958) p. 539.
24. P. VILLARS and L. D. CALVERT, in "Pearson's Handbook of Crystallographic Data for Intermetallic Phases, Volume 2" (American Society for Metals, Metals Park, OH, 1985) p. 1877.
25. L. WANG and R. D. PEHLKE, *Met. Trans.* **19B** (1988) 471.
26. M. KAJIHARA, M. KIKUCHI and S. K. CHOI, in "Proceedings of Phase Transformations '87 Conference", University of Cambridge (The Institute of Metals, London, 1988) p. 265.
27. D. B. RAYAPROLU and A. HENDRY, *Mater. Sci. Technol.* **5** (1989) 328.
28. M. HILLERT, *Acta Metall.* **30** (1982) 1689.
29. O. HAMMAR and U. SVENSSON, in "Solidification and Casting of Metals", Proceedings of an International Conference on Solidification, University of Sheffield, July 1977, Session 6: Structure and Property Relationships and Welding, edited by A. G. Fuller (The Metals Society, London, 1979) p. 401.
30. K. FRISK and M. HILLERT, in "Proceedings of the International Conference on High Nitrogen Steels, HNS 88", Lille, France, May 1988, edited by J. Foct and A. Hendry (The Institute of Metals, London, 1989) p. 1.